

Spectroscopic Determination of Proton Position in the Proton-Coupled Electron Transfer Pathways of Donor–Acceptor Supramolecule Assemblies

Joel Rosenthal, Justin M. Hodgkiss, Elizabeth R. Young, and Daniel G. Nocera*

Contribution from the Department of Chemistry, 6-335, Massachusetts Institute of Technology, 77 Massachusetts Avenue, Cambridge, Massachusetts 02139-4307

Received April 8, 2006; E-mail: nocera@mit.edu

Abstract: A homologous set of porphyrin derivatives possessing an isocyclic five-membered ring appended with an amidinium functionality has been used to examine proton-coupled electron transfer (PCET) through well-characterized amidine–carboxylic acid interfaces. Conjugation between the porphyrin chromophore and the amidinium interface can be altered by selective reduction of the isocyclic ring of an amidinium–purpurin to produce an amidinium–chlorin. The highly conjugated amidinium–purpurin displays large spectral shifts in the visible region upon alteration of the amidinium/amidine protonation state; no such change is observed for the chlorin homologue. Analysis of the UV–vis absorption and emission profiles of the amidinium–purpurin upon deprotonation allows for the measurement of the porphyrinic–amidinium acidity constant for the ground state ($pK_a = 9.55 \pm 0.1$ in CH_3CN) and excited state ($pK_a^* = 10.40 \pm 0.1$ in CH_3CN). The absorption spectrum of the purpurin also provides a convenient handle for determining the protonation state of assembled interfaces. In this way, the purpurin macrocycle provides a general tool for PCET studies because it can be used to determine the location of a proton within PCET interfaces formed from carboxylic acid electron acceptors including dinitrobenzenes (DNBs) and naphthalenediimide (NI), which have been used extensively in previous PCET studies. An amidine–carboxylic acid interface is observed for electron-rich acceptors, whereas the ionized amidinium–carboxylate interface is observed for electron-poor acceptors. The PCET kinetics for purpurin/chlorin associated to NI are consistent with an amidine–carboxylic acid interface, which is also verified spectrally.

Introduction

The effect of proton motion on electron transfer (ET) has been investigated by combining the strategy of photoinduced fixed-distance ET with that for photoinduced proton transfer.^{1–3} The approach relies on the construction of donor–acceptor (D–A) pairs juxtaposed by proton transfer interfaces [H^+] formed from carboxylic acid dimers,^{4,5} guanine–cytosine base-pairs,⁶ and amidinium–carboxylate salt bridges.^{7–10} The proximal [H^+] interface exerts its greatest influence on the PCET event when it is asymmetric and capable of supporting proton

transfer. The charge shift resulting from the motion of the proton can couple to the charge shift of the electron transfer through the polarization of the surrounding environment.^{2,11–21} It is this mechanism that distinguishes ET from PCET.

The overall kinetics of the PCET reaction is dictated by the protonation state of the interface. For instance, consider the two tautomeric forms of nonionized amidine–carboxylic acid and amidinium–carboxylate salt-bridge interfaces shown in Chart 1. The PCET kinetics will differ significantly for an electron that traverses the neutral interface versus the charged interface, owing to disparate coupling to the polarization of the surrounding medium. Charge separation will be mitigated by proton motion in the salt bridge, whereas charge separation across the

- (1) Chang, C. J.; Brown, J. D. K.; Chang, M. C. Y.; Baker, E. A.; Nocera, D. G. In *Electron Transfer in Chemistry*; Balzani, V., Ed.; Wiley-VCH: Weinheim, Germany, 2001; Vol. 3.2.4, pp 409–461.
- (2) Cukier, R. I.; Nocera, D. G. *Annu. Rev. Phys. Chem.* **1998**, *49*, 337–369.
- (3) Chang, C. J.; Chang, M. C. Y.; Damrauer, N. H.; Nocera, D. G. *Biochim. Biophys. Acta* **2004**, *1655*, 13–28.
- (4) Turró, C.; Chang, C. K.; Leroi, G. E.; Cukier, R. I.; Nocera, D. G. *J. Am. Chem. Soc.* **1992**, *114*, 4013–4015.
- (5) de Rege, P. J. F.; Williams, S. A.; Therien, M. J. *Science* **1995**, *269*, 1409–1413.
- (6) Sessler, J. L.; Wang, B.; Springs, S. L.; Brown, C. T. In *Comprehensive Supramolecular Chemistry*; Murakami, Y., Ed.; Pergamon Press: Oxford, 1996; Vol. 4, pp 311–336, and references therein.
- (7) Damrauer, N. H.; Hodgkiss, J. M.; Rosenthal, J.; Nocera, D. G. *J. Phys. Chem. B* **2004**, *108*, 6315–6321.
- (8) Roberts, J. A.; Kirby, J. P.; Nocera, D. G. *J. Am. Chem. Soc.* **1995**, *117*, 8051–8052.
- (9) Roberts, J. A.; Kirby, J. P.; Wall, S. T.; Nocera, D. G. *Inorg. Chim. Acta* **1997**, *263*, 395–405.
- (10) Kirby, J. P.; Roberts, J. A.; Nocera, D. G. *J. Am. Chem. Soc.* **1997**, *119*, 9230–9236.

- (11) Cukier, R. I. *J. Phys. Chem.* **1996**, *100*, 15428–15443.
- (12) Cukier, R. I. *J. Phys. Chem.* **1994**, *98*, 2377–2381.
- (13) Zhou, X. G.; Cukier, R. I. *J. Phys. Chem.* **1995**, *99*, 945–954.
- (14) Cukier, R. I. *J. Phys. Chem. A* **1999**, *103*, 5989–5995.
- (15) Cukier, R. I. *Biochim. Biophys. Acta* **2004**, *1655*, 37–44.
- (16) Hammes-Schiffer, S. In *Electron Transfer in Chemistry*; Balzani, V., Ed.; Wiley-VCH: Weinheim, Germany, 2001; Vol. 1.1.5, p 189.
- (17) Hammes-Schiffer, S. *Acc. Chem. Res.* **2001**, *34*, 273–281.
- (18) Hammes-Schiffer, S.; Iordanova, N. *Biochim. Biophys. Acta* **2004**, *1655*, 29–36.
- (19) Soudackov, A.; Hammes-Schiffer, S. *J. Chem. Phys.* **1999**, *111*, 4672–4687.
- (20) Soudackov, A.; Hammes-Schiffer, S. *J. Chem. Phys.* **2000**, *113*, 2385–2396.
- (21) Decornez, H.; Hammes-Schiffer, S. *J. Phys. Chem. A* **2000**, *104*, 9370–9384.

Chart 1

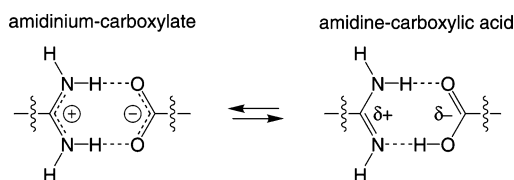
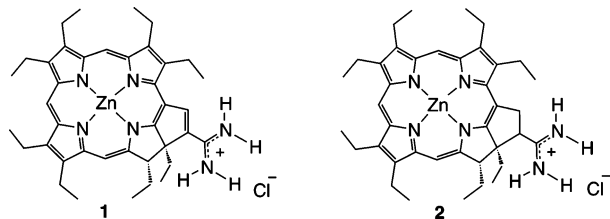


Chart 2



neutral interface will develop with proton motion. Moreover, the driving force for ET through the two interfaces will be differentiated by virtue of the pK_a dependence of the redox potentials of the donor and acceptor. Finally, the hydrogen bond strength and accordingly the electronic coupling may differ for both tautomers. Given that all the essential factors that control a PCET reaction are perturbed by the charge distribution within the proton transfer network, knowledge of the electronic structure of the interface is essential to a thorough understanding of PCET mechanism. Nonetheless, for all PCET model systems studied to date, the charge distribution within the interface has remained ill-defined owing to the absence of spectroscopic signatures that can be used to determine the proton position. We now report the construction of purpurin **1** (Chart 2), in which conjugation between an amidinium functionality and the macrocyclic chromophore permits the location of the proton within the interface to be ascertained by monitoring wavelength shifts of the Soret and Q-bands of the purpurin framework. The purpurin macrocycle provides a general tool for PCET studies because it can be used to probe which tautomer prevails for carboxylic acid electron acceptors including dinitrobenzenes (DNBs) and naphthalenediimide (NI), which have been used extensively in previous PCET studies. Purpurin **1** provides the added benefit that the electronic communication between the interface and the electron donor–acceptor pair may be conveniently examined. Reduction of the five-membered isocyclic ring of **1** yields chlorin **2** (Chart 2). Unlike **1**, the absorption spectrum of **2** is invariant with pH. Accordingly, homologous derivatives **1** and **2** permit PCET kinetics to be compared for a D–[H⁺]–A assembly in which electronic communication between the proton interface and electron donor–acceptor sites is turned on and off.

Experimental Section

Materials. Silica gel 60 (70–230 and 230–400 mesh, Merck) and Merck 60 F254 silica gel (precoated sheets, 0.2 mm thick) were used for column and analytical thin-layer chromatography, respectively. Solvents for synthesis were of reagent grade or better and were dried according to standard methods.²² Spectroscopic experiments employed THF or CH₃CN (spectroscopic grade), which were also dried according to standard methods²² and stored under vacuum. Mass spectral analyses were performed in the MIT Department of Chemistry Instrumentation

Facility (DCIF) or at the University of Illinois Mass Spectrometry Laboratory. Ni(II) 2,3,7,8,12,13,17,18-octaethylporphyrin (**3**)²³ and [N-(1-(2,5-di-*tert*-butylphenyl))-N'-(1-(carboxymethyl)naphthalene-1,8:4,5-tetracarboxydimide)]TMA (**NI**)⁷ were prepared using published procedures.

Physical Measurements. ¹H NMR spectra were recorded at 25 °C in the MIT DCIF on a Varian XL-300, Unity 300, or Mercury 300 spectrometer. All chemical shifts are reported using the standard δ notation in parts-per-million; positive chemical shifts are to higher frequency from the given reference. Absorption spectra were obtained using either a Cary-17 spectrophotometer modified by On-Line Instrument Systems (OLIS) to include computer control or a Spectral Instruments 440 Series spectrophotometer.

Samples for lifetime measurements were contained within a high-vacuum cell consisting of a 2-mm path length clear fused-quartz cell (Starna cells), which was connected to a 10-cm³ solvent reservoir via a graded seal. The two chambers were isolated from the environment and from each other by high-vacuum Teflon valves. An aliquot of purpurin or chlorin ($\sim 6 \times 10^{-8}$ mol) was added to the cell, and in experiments employing the **NI** acceptor or benzoate, the required equivalents were initially added to the solvent reservoir. The transferring solvent was removed from both compartments on a high-vacuum manifold (10⁻⁵ Torr). Dry THF was subject to at least three freeze–pump–thaw cycles (10⁻⁵ Torr) and added to the cell by vacuum transfer to make a 60 μ M solution of the purpurin or chlorin with an optical density of ~ 0.3 at the Q₀₀ absorption band. In this configuration, the spectroscopy on the purpurin or chlorin was examined initially. By opening the valve between the two compartments, the spectroscopy of associated complexes could be performed while maintaining high vacuum and exactly the same amount of compound and solvent.

The excitation source for luminescence lifetime measurements was a chirped-pulse amplified Ti:Sapphire laser system that has been described elsewhere.⁷ In this experiment, the 100 fs, 800 nm output of the regenerative amplifier was frequency-upconverted in a visible optical parametric amplifier (BMI Alpha-1000) to produce excitation pulses at 660 nm for resonant excitation of the Q-band of purpurin **1** or 620 nm for resonant excitation of chlorin **2**. The excitation was vertically polarized and attenuated to 100–200 nJ/pulse. Luminescence lifetime kinetics were measured on a Hamamatsu C4334 Streak Scope streak camera. The emission was collected at the magic angle ($\theta_m = 54.7^\circ$) over a 140 nm window centered on the emission peak.

Samples of Ni(II) purpurin **9** used for absorption spectroscopy were prepared in the same way as described for lifetime measurements (above), except that high-vacuum cells with 1 cm path length were used, and a purpurin/chlorin concentration of 15 μ M was employed to give an optical density of ~ 1.0 at the Soret absorption band and ~ 0.30 at the Q₀₀ absorption band.

A Benesi–Hildebrand plot was developed for the spectral shift of the Soret band ($1/\Delta A_{423}$ vs $1/[L]$) of purpurin **9** upon its titration with 4-(dimethylamino)pyridine (DMAP). The deprotonation constant K_a' for the purpurin amidinium is obtained from the ratio of the y-intercept and slope.²⁴ The DMAP titration was performed in a 1-cm high-vacuum cell. Purpurin **9** was added to the cell and the transferring solvent removed with a high-vacuum manifold (10⁻⁵ Torr). Dry acetonitrile was subject to at least three freeze–pump–thaw cycles (10⁻⁵ Torr) and added to the cell by vacuum transfer. Prior to each addition of DMAP (total equivalents DMAP = 40, 80, 180, 280, 380, and 480), the acetonitrile was vacuum transferred to the cuvette with a dry ice/acetone bath and sealed from the solvent reservoir and environment. This procedure ensured that the solvent volume remained constant throughout the course of the experiment. A stock solution of DMAP was added to the open solvent reservoir, while preserving the vacuum

(23) Paine, J. B., III; Kirshner, W. B.; Moskowitz, D. W. *J. Org. Chem.* **1976**, *41*, 3857–3860.

(24) Connors, K. A. In *Binding Constants: A Measurement of Molecular Complex Stability*; Wiley: New York, 1987.

(22) Armarego, W. L. F.; Perrin, D. D. *Purification of Laboratory Chemicals*, 4th ed.; Butterworth-Heinemann: Oxford, 1996.

in the cuvette, and the transferring solvent was removed with a high-vacuum manifold (10^{-5} Torr). The solvent reservoir was then sealed from the environment and opened to the cuvette compartment to introduce each new addition of DMAP. Additional titrations of purpurin **9** were performed with *n*-tetrabutylammonium (TBA) benzoate, 2,4- and 3,5-dinitrobenzoate, and phenylsulfonate in dichloromethane following the procedure outlined above using a 2-mm cell.

Electrochemical experiments were carried out using a Bioanalytical Systems (BAS) Model CV-50W potentiostat/galvanostat. Cyclic voltammetry and differential pulse voltammetry were performed in a two-compartment cell using a platinum disk as the working electrode, a Ag/AgCl reference electrode, and a platinum wire auxiliary electrode. The supporting electrolyte used for electrochemistry experiments was either 0.1 M *n*-tetrabutylammonium hexafluorophosphate (TBAPF₆) or perchlorate (TBAP). The solution in the working compartment of the cell was deaerated by a nitrogen stream. Background cyclic voltammograms of the electrolyte solution were recorded prior to addition of the solid sample. Redox couples were referenced to SCE by using a ferrocenium/ferrocene internal standard of 0.307 V vs SCE.²⁵

X-ray diffraction experiments were performed on single crystals grown by a slow diffusion of methanol into a concentrated methylene chloride solution of **7** at room temperature. Crystals were removed from the supernatant liquid and transferred onto a microscope slide coated with Paratone N oil. Selected crystals were affixed to a glass fiber in wax and Paratone N oil and cooled to 173 K. Data collection was performed by shining Mo K α ($\lambda = 0.71073$ Å) radiation with a frame time of 45 s and a detector distance of 4.9 cm onto crystals mounted on a three-circle goniometer Siemens Platform equipped with a CCD detector. The data were processed and refined by using the program SAINT supplied by Siemens Industrial Automation. The structure was solved and refined by direct methods (SHELXTL v6.12, Sheldrick, G. M., and Siemens Industrial Automation, 2000) in conjunction with standard difference Fourier techniques. All non-hydrogen atoms were refined anisotropically. Hydrogen atoms were placed in calculated positions. Some details regarding the refined data and cell parameters are provided in Table 1.

Computations. Density functional theory calculations (DFT) were performed using the Amsterdam Density Functional (ADF2002.02) program^{26,27} on a home-built Linux cluster comprising 60 Intel processors organized in groups of 12 running in parallel. The generalized gradient approximation was used as implemented in ADF by the Becke-88 functional for exchange²⁸ and the Perdew-Wang-91 functional for correlation.²⁹ A basis set of triple- ζ Slater-type functions augmented by a polarization set (TZP) was used for Zn and N atoms and double- ζ with polarization (DZP) for other atoms, with the frozen core approximation. Orbitals were visualized using the Molekel v.4.2 Linux-mesa software.^{30,31}

The electrostatic stabilization energy of 0.5 eV was calculated for the amidinium-carboxylate salt bridge at a distance of $r = 3.9$ Å⁷ in THF. This distance is measured between the central carbon atoms of the amidinium and carboxylate groups from the energy-optimized structure. The Coulombic interaction was determined for the point charges, q_1 and q_2 , according to $V = (q_1q_2)/(4\pi\epsilon r)$ where ϵ is the dielectric constant of the medium (7.58 for THF³²).

Table 1. Summary of X-ray Crystallography Data for **7**

empirical formula	C ₃₉ H ₄₇ N ₅
fw	585.82
temperature	173(2) K
wavelength	0.71073 Å
cryst syst	triclinic
space group	$P\bar{1}$
unit cell dimens	$a = 10.6710(16)$ Å, $\alpha = 78.040(3)^\circ$ $b = 12.0211(18)$ Å, $\beta = 78.255(3)^\circ$ $c = 13.823(2)$ Å, $\gamma = 70.890(3)^\circ$
volume	1621.4(4) Å ³
Z	2
density (calcd)	1.200 Mg/m ³
absorb coeff	0.071 mm ⁻¹
$F(000)$	632
cryst size	0.35 × 0.35 × 0.07 mm ³
θ range for data collection	1.52 to 25.09°
index ranges	$-12 < h < 12$, $-13 < k < 14$, $0 < l < 16$
no. of reflns collected	10 490
no. of indep reflns	5680 [$R_{int} = 0.0292$]
completeness to $\theta = 28.34^\circ$	98.6%
absorb corr	multiscans
refinement method	full-matrix least-squares on F^2
no. of data/restraints/params	5680/106/489
goodness-of-fit on F^2	1.028
final R indices [$I > 2\sigma(I)$] ^a	$R_1 = 0.0516$, $wR_2 = 0.1343$
R indices (all data) ^a	$R_1 = 0.0746$, $wR_2 = 0.1533$
largest diff peak and hole	0.711 and -0.234 e/Å ⁻³

^a $R_1 = \sum ||F_o| - |F_c|| / \sum |F_o|$, $wR_2 = (\sum (w(F_o^2 - F_c^2)^2) / \sum (w(F_o^2)^2))^{1/2}$, $GOF = (\sum w(F_o^2 - F_c^2)^2 / (n - p))^{1/2}$ where n is the number of data and p is the number of parameters refined.

Nickel(II) meso-Formyl-2,3,7,8,12,13,17,18-octaethylporphyrin (4). A suspension of **3** (500 mg, 0.845 mmol) in 300 mL of anhydrous 1,2-dichloroethane was added over a period of 10 min under nitrogen to a warm solution (50–60 °C) of Vilsmeier reagent, prepared from anhydrous dimethyl formamide (DMF) (2.7 mL, 34.5 mmol) and freshly distilled POCl₃ (2.7 mL, 34.5 mmol). The reaction temperature was maintained at 50–60 °C for 15 min and was then warmed to 75 °C under nitrogen for 1 h. The reaction was quenched by the addition of 200 mL of a saturated solution of Na₂CO₃, and the resulting mixture was stirred at 75 °C for an additional 2 h under air. The organic phase was then decanted and the aqueous phase was twice extracted with CH₂Cl₂ (75 mL). All organic extracts were combined, washed with water, and dried over Na₂SO₄. Following removal of solvent, purification by column chromatography on silica using CH₂Cl₂ and hexanes as the eluent (3:1) afforded the title compound (444 mg, 85% yield). ¹H NMR (300 MHz, CDCl₃, 25 °C), δ /ppm: 9.30 (s, 1H), 9.27 (s, 2H), 3.70 (m, 16H), 1.70 (m, 24H). ESIMS [M + H]⁺, m/z : calcd for C₃₇H₄₄N₄NiO, 619.2950; found, 619.2956.

Nickel(II) meso-(β -Cyanoethenyl)-2,3,7,8,12,13,17,18-octaethylporphyrin (5). To a suspension of NaH (0.24 g, 10.0 mmol, 60% dispersion in mineral oil) in dry THF (10 mL) under a nitrogen atmosphere was added diethyl cyanomethylphosphonate (1.0 g, 5.65 mmol) at ambient temperature. A solution of **4** (1.0 g, 1.62 mmol) in 20 mL of dry THF was transferred to the NaH suspension via syringe. The resultant solution was heated at reflux under a nitrogen atmosphere for 1.5 h and then cooled to room temperature. The solution was diluted with CH₂Cl₂ (100 mL) and washed three times with water (75 mL). The organic layer was collected and dried over Na₂SO₄, and the solvent removed under reduced pressure. The resulting purple material was purified by column chromatography on silica using CH₂Cl₂ and hexanes as the eluent (1:1). The resulting solid was redissolved in a minimal amount of CH₂Cl₂ and precipitated by addition of CH₃OH to afford purple microcrystals of **5** (0.91 g) in 87% yield. ¹H NMR (300 MHz, CDCl₃, 25 °C), δ /ppm: 9.72 (d, 1H), 9.41 (br s, 3H), 4.58 (d, 1H),

(25) Bard, A. J.; Faulkner, L. R. *Electrochemical Methods. Fundamentals and Applications*; John Wiley: New York, 1980.

(26) te Velde, G.; Bickelhaupt, F. M.; van Gisbergen, S. J. A.; Fonseca Guerra, C.; Baerends, E. J.; Snijders, J. G.; Ziegler, T. J. *Comput. Chem.* **2001**, *22*, 931–967.

(27) Fonseca Guerra, C.; Snijders, J. G.; te Velde, G.; Baerends, E. J. *Theor. Chem. Acc.* **1998**, *99*, 391–403.

(28) Becke, A. D. *Phys. Rev. A* **1988**, *38*, 3098–3100.

(29) Perdew, J. P.; Chevary, J. A.; Vosko, S. H.; Jackson, K. A.; Pederson, M. R.; Singh, D. J.; Fiolhais, C. *Phys. Rev. B* **1992**, *46*, 6671–6687.

(30) Flükiger, P.; Lüthi, H. P.; Portmann, S.; Weber, J. *Molekel v.4.2/3*; Swiss Center for Scientific Computing: Manno (Switzerland), 2000–2002.

(31) Portmann, S.; Lüthi, H. P. *Chimia* **2000**, *54*, 766–769.

(32) Marcus, Y. In *Ion Solvation*; John Wiley and Sons: Chichester, 1985; p 136.

3.78 (m, 16H), 1.75 (m, 24H). ESIMS $[M]^+$, m/z : calcd for $C_{39}H_{45}N_5Ni$, 641.3028; found, 641.3049.

meso-(β -Cyanoethenyl)-2,3,7,8,12,13,17,18-octaethylporphyrin (6). To a solution of the Ni(II) complex **5** (500 mg, 0.78 mmol) in 80 mL of CH_2Cl_2 was added concentrated sulfuric acid (15 mL), and the biphasic mixture was stirred under air at ambient temperature until all of the porphyrin was extracted into the sulfuric acid layer. The reaction mixture was poured onto 50 g of ice and neutralized with saturated aqueous sodium carbonate. Following neutralization, the organic layer was collected, washed with water, dried over Na_2SO_4 , and concentrated under reduced pressure. Purification was accomplished by column chromatography on silica using CH_2Cl_2 and hexanes as the eluent (2:1). The resulting solid was redissolved in a minimal amount of CH_2Cl_2 and precipitated by addition of CH_3OH to afford **6** (450 mg) in 98% yield. 1H NMR (300 MHz, $CDCl_3$, 25 °C), δ /ppm: 10.06 (d, 1H), 10.04 (s, 1H) 9.96 (s, 2H), 5.58 (d, 1H), 4.01 (m, 16H), 1.79 (m, 24H), -3.14 (s, 2H). ESIMS $[M + H]^+$, m/z : calcd for $C_{39}H_{47}N_5$, 586.3904; found, 586.3918.

Cyano-2,3,7,8,12,13,17,18-octaethylpurpurin (7). Porphyrin **6** (450 mg, 0.78 mmol) was dissolved in 80 mL of glacial acetic acid, and the resultant solution was heated at reflux under a nitrogen atmosphere for 24 h. The solvent was removed under reduced pressure and the residue dissolved in CH_2Cl_2 . Chromatography on silica gel using CH_2Cl_2 as the eluent yielded a major green fraction, which was collected and concentrated in vacuo. The resulting solid was redissolved in a minimal amount of CH_2Cl_2 and precipitated by addition of CH_3OH to afford purple microcrystals of purpurin **7** (370 mg) in 81% yield. 1H NMR (300 MHz, $CDCl_3$, 25 °C), δ /ppm: 9.51 (s, 1H), 9.48 (s, 1H), 9.20 (s, 1H), 8.49 (s, 1H), 3.80 (m, 12H), 2.95 (m, 2H) 2.50 (m, 2H), 1.75 (m, 21H), -0.22 (t, 3H), -0.45 (s, 1H), -1.05 (s, 1H). ESIMS $[M + H]^+$, m/z : calcd for $C_{39}H_{47}N_5$, 586.3904; found, 586.3913.

Nickel(II) Purpurin Nitrile (8). To a solution of purpurin **7** (200 mg, 0.341 mmol) in 15 mL of DMF was added a large excess of $Ni(OAc)_2 \cdot (H_2O)_4$. The mixture was heated at reflux under a nitrogen atmosphere until chelation of the metal ion by the macrocycle was complete, as monitored by UV-vis spectroscopy and TLC (~1 h). The solution was then cooled to room temperature, diluted with 200 mL of water, and extracted twice with 75 mL of CH_2Cl_2 . The organic extracts were combined, washed several times with water, dried over Na_2SO_4 , and then concentrated under reduced pressure. Purification on silica using CH_2Cl_2 as the eluent gave **8** (202 mg) in 92% yield. 1H NMR (300 MHz, $CDCl_3$, 25 °C), δ /ppm: 9.02 (s, 2H), 8.80 (s, 1H), 7.79 (s, 1H), 3.78 (m, 1H), 3.55 (m, 13H), 2.65 (m, 2H) 2.04 (m, 2H), 2.80 (m, 2H), 1.65 (m, 21H), -0.10 (t, 3H). ESIMS $[M + H]^+$, m/z : calcd for $C_{39}H_{45}N_5Ni$, 642.3101; found, 642.3039.

Nickel(II) Purpurin Amidinium Chloride (9). To a toluene solution (50 mL) of **8** (100 mg, 0.155 mmol) was added chloromethylaluminum amide (4.0 mL, 1.2 M in toluene) under a nitrogen atmosphere. The reaction solution was heated at 90 °C under nitrogen for 3 days. The resulting solution was then cooled to room temperature, poured slowly onto a slurry of silica gel (15 g) in $CHCl_3$ (30 mL), and stirred under air for 10 min. The slurry was filtered over sintered glass, and the filtercake was washed with CH_2Cl_2/CH_3OH (3:1) until all porphyrin product had been eluted. The filtrate was concentrated under reduced pressure, and the residue purified by column chromatography on silica using CH_2Cl_2/CH_3OH (20:1) as the eluent to yield **9** (83 mg, 81%). 1H NMR (300 MHz, $CDCl_3$, 25 °C), δ /ppm: 9.20 (s, 1H), 9.12 (s, 1H), 9.10 (s, 1H), 8.96 (br, 2H), 8.81 (br, 2H), 8.19 (s, 1H) 4.03 (m, 1H), 3.62 (m, 13H), 2.81 (m, 2H), 2.66 (m, 2H), 1.57 (m, 21H), -0.21 (t, 3H). FABMS $[M - Cl]^+$, m/z : calcd for $C_{39}H_{49}N_6Ni$, 659.3372; found, 659.3372.

Zinc(II) Purpurin Amidinium Chloride (1). Concentrated H_2SO_4 (5 mL) was added to an ice cold stirred solution of **9** (80 mg, 0.12 mmol) in 150 mL of CH_2Cl_2 . This mixture was stirred at 0 °C until all of the porphyrinic material had been extracted into the acid layer, at which point, 50 g of ice was added. Neutralization of the acidic mixture

was accomplished by slowly adding an aqueous solution of saturated sodium bicarbonate. Following neutralization, the organic phase was separated, and the aqueous layer was twice washed by CH_2Cl_2 (75 mL). The organic extracts were combined, dried over Na_2SO_4 , and concentrated under reduced pressure. Without further purification, the free-base purpurin was dissolved in $CHCl_3$ (20 mL), and $ZnCl_2$ (136 mg, 1.0 mmol) dissolved in a minimal amount of CH_3OH was added to the stirred solution. The reaction mixture was heated at reflux under an atmosphere of nitrogen for 1 h and then concentrated under vacuum. Water was added to the concentrate, which was twice extracted with CH_2Cl_2 (40 mL). The crude product was purified by column chromatography on silica using CH_2Cl_2/CH_3OH (10:1) as the eluent to yield the title compound (62 mg, 77%). FABMS $[M - Cl]^+$, m/z : calcd for $C_{39}H_{49}N_6Zn$, 665.3310; found, 665.3311.

Chlorin Nitrile (10). Palladium on charcoal (Pd/C) (10%, 20 mg) was added to a stirred solution of purpurin nitrile **7** (120 mg, 0.20 mmol) in dry THF (20 mL) containing triethylamine (0.1 mL). The resulting mixture was hydrogenated at room temperature under a slightly positive pressure of hydrogen gas. After stirring the suspension under hydrogen for 12 h, the reaction mixture was filtered and the resultant solution was stirred vigorously under air. Following the complete reoxidation of the intermediate porphyrinogen, which was followed by measuring the increasing intensity of an absorption band at 660 nm in the UV-vis spectrum, the solvent was removed in vacuo, and the resultant material purified by chromatography on silica using CH_2Cl_2/CH_3OH (100:1). The major blue band was collected, the solvent removed under reduced pressure, and the crude product recrystallized from CH_2Cl_2/CH_3OH (100:1) to give the title compound (88 mg, 75% yield). 1H NMR (300 MHz, $CDCl_3$, 25 °C), δ /ppm: 9.60 (s, 2H), 8.45 (s, 1H), 5.04 (m, 1H), 5.02 (m, 1H), 4.30 (m, 1H), 4.15 (m, 1H) 3.85 (m, 12H), 2.80 (m, 2H), 2.10 (m, 2H) 1.75 (m, 21H), -0.31 (t, 3H), -1.70 (s, 1H), -2.35 (s, 1H). ESIMS $[M + H]^+$, m/z : calcd for $C_{39}H_{49}N_5$, 588.4061; found, 588.4075.

Nickel(II) Chlorin Nitrile (11). Ni(II) was inserted into the macrocycle of **10** following the same procedure described for the preparation of **8** to generate 60 mg of **11** (87% yield). 1H NMR (300 MHz, $CDCl_3$, 25 °C), δ /ppm: 9.09 (s, 2H), 7.65 (s, 1H), 4.83 (m, 1H), 4.41 (m, 1H), 3.90 (m, 1H), 3.82 (m, 1H), 3.54 (m, 12H), 2.65 (m, 2H) 2.31 (m, 2H), 1.86 (m, 2H), 1.62 (m, 21H), 0.16 (t, 3H). ESIMS $[M]^+$, m/z : calcd for $C_{39}H_{47}N_5Ni$, 643.3179; found, 643.3198.

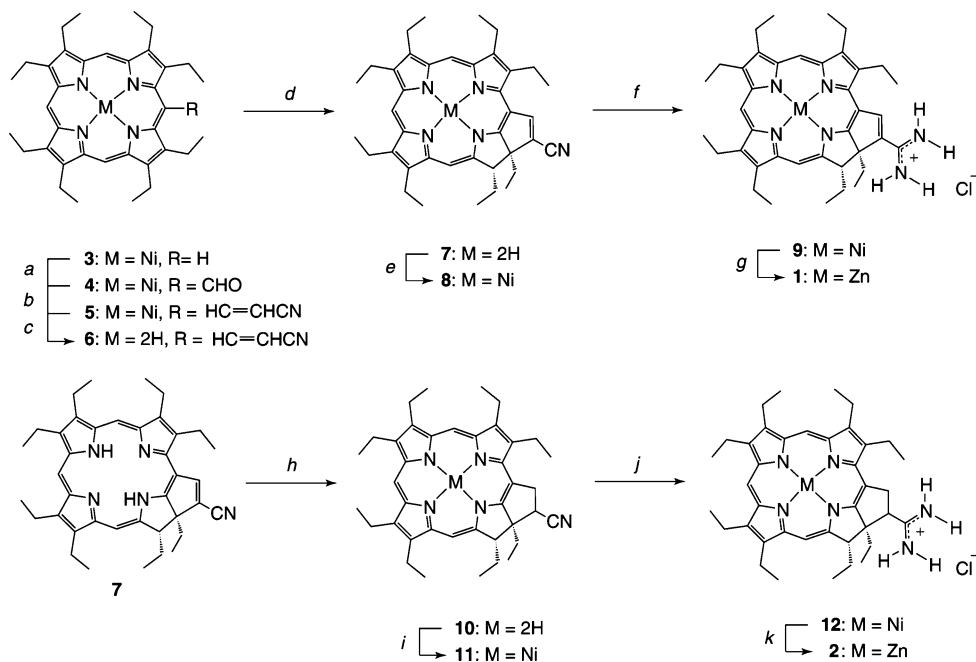
Nickel(II) Chlorin Amidinium Chloride (12). The nitrile of **11** was converted to amidinium using a procedure identical to that used for purpurin **9** to generate 47 mg of the title compound (84% yield). 1H NMR (300 MHz, $CDCl_3$, 25 °C), δ /ppm: 9.10 (br, 2H), 9.05 (s, 1H), 9.00 (s, 1H), 7.55 (s, 1H), 6.95 (br, 2H), 4.15 (m, 1H), 3.82 (m, 1H) 3.70 (m, 1H), 3.65 (m, 1H), 3.50 (m, 12H), 1.80 (m, 2H), 1.70 (m, 2H), 1.61 (m, 21H), -0.50 (t, 3H). ESIMS $[M - Cl]^+$, m/z : calcd for $C_{39}H_{49}N_6Ni$, 661.3523; found, 661.3524.

Zinc(II) Chlorin Amidinium Chloride (2). Ni(II) demetalation of **12** and Zn(II) insertion was accomplished using a procedure identical to that used for purpurin **1** to generate 30 mg of the title compound (62% yield). FABMS $[M - Cl]^+$, m/z : calcd for $C_{39}H_{49}N_6Zn$, 667.3467; found, 667.3247.

Results

The synthetic strategy used to derivatize the homologous purpurin and chlorin macrocycles with amidinium functionalities is presented in Scheme 1. The amidinium purpurin and chlorin are delivered by a method employed previously for the preparation of amidinium porphyrins, namely, the conversion of the nitrile to the amidinium conjugate using Weinreb's amide transfer reagent.³³ For both purpurin amidinium **1** and chlorin amidinium **2**, Ni(II) 2,3,7,8,12,13,17,18-octaethylporphyrin

(33) Levin, J. I.; Turos, E.; Weinreb, S. M. *Synth. Commun.* **1982**, *12*, 989–993.

Scheme 1^a

^a (a) Vilsmeier reagent, 1,2-dichloroethane; (b) NaH, (EtO)₂P(O)CH₂CN; (c) H₂SO₄; (d) AcOH, reflux; (e) H₂SO₄; (f) AlCl(CH₃)(NH₂), toluene; (g) 1. H₂SO₄; 2. ZnCl₂, CHCl₃, CH₃OH; (h) H₂, Pd/C; (i) Ni(OAc)₂, DMF; (j) AlCl(CH₃)(NH₂), toluene; (k) 1. H₂SO₄; 2. ZnCl₂, CHCl₃, CH₃OH.

(NiOEP) (**3**) was the chosen starting material due to the advantageous solubilizing properties of the β -ethyl groups. Formylation of **3** using Vilsmeier's reagent proceeds smoothly to deliver NiOEP aldehyde **4**.³⁴ Treatment of cyanomethylphosphonate with sodium hydride generates a Wittig reagent, which reacts with **4** to afford *meso*-(β -cyanoethenyl)porphyrin **5**. Demetalation with concentrated H₂SO₄ yields free-base porphyrin **6**, which followed by cyclization in refluxing glacial acetic acid, affords the corresponding cyano-2,3,7,8,12,13,17,18-octaethylpurpurin (**7**) in high yield. The use of the free-base porphyrin is essential to fusing the five-membered ring to the macrocycle because the initial cyclization step is promoted by protonation of the porphyrin nitrogen.³⁵

Mass spectrometry of uncyclized **6** and cyclized **7** clearly shows the compounds to be isomers. The cyclization of **6** to **7** may be easily monitored in the ¹H NMR. The signals associated with the acrylate protons of **6** (doublets at $\delta = 5.58$ and 10.06 ppm) are replaced by a singlet ($\delta = 9.20$ ppm) that is ascribed to the olefinic proton of the isocyclic cyclopentenyl ring in the cyclized product. Of the three *meso* protons, the one shifted upfield by approximately 1 ppm identifies its placement adjacent to a reduced pyrrole ring.³⁶ Additionally, both methyl and methylene resonances of a peripheral ethyl group exhibit upfield shifts of approximately 1 ppm, consistent with their position ancillary to the nonplanar and reduced pyrrole ring.³⁷

Details of the structure of the purpurin core were provided by cyano purpurin **7**. The thermal ellipsoid plot of the X-ray crystal structure of **7** shown in Figure 1 is similar to that of other porphyrinic derivatives with partially reduced pyrrole subunits.^{38–45} Specific hydrogen atoms of interest, including those localized on opposite pyrrole rings as well as that on the

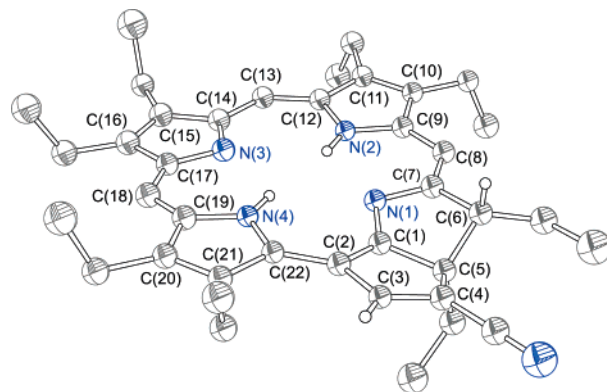


Figure 1. Solid-state structure of **7** with thermal ellipsoids shown at the 50% probability level.

pyrrole ring adjacent to the isocyclic five-membered ring, are shown in Figure 1. Cyano purpurin **7** is largely planar, except for the sp³-hybridized tetrahedral center adjacent to the isocyclic five-membered ring on the macrocycle periphery (Figure 1). The presence of the five-membered ring fused to the edge of the porphyrin macrocycle has several structural consequences: (1) The existence of this tetrahedral center results in **7** being chiral; in the solid state, purpurin **7** crystallizes with both

(34) Morgan, A. R.; Tertel, N. C. *J. Org. Chem.* **1986**, *51*, 1347–1350.
 (35) Woodward, R. B. In *Selected Organic Syntheses*; Fleming, I., Ed.; John Wiley: New York, 1973; pp 112–114.
 (36) Bonnett, R.; Stephenson, G. F. *Chem. Commun.* **1966**, 1600–1601.
 (37) Chang, C. K. *Biochemistry* **1980**, *19*, 1971–1976.

(38) Jaquinod, L.; Gros, C.; Khoury, R. G.; Smith, K. M. *Chem. Commun.* **1996**, 2581–2582.
 (39) Jaquinod, L.; Nurco, D. J.; Medforth, C. J.; Ravindra, K. P.; Forsyth, T. P.; Olmstead, M. M.; Smith, K. M. *Angew. Chem., Int. Ed. Engl.* **1996**, *35*, 1013–1016.
 (40) Simonneaux, G.; Kobeissi, M.; Toupet, L. *Inorg. Chem.* **2003**, *42*, 1644–1651.
 (41) Richeter, S.; Jeandon, C.; Gisselbrecht, J.-P.; Ruppert, R.; Callot, H. J. *J. Am. Chem. Soc.* **2002**, *124*, 6168–6179.
 (42) Balasubramanina, T.; Strachan, J.-P.; Boyle, P. D.; Lindsey, J. S. *J. Org. Chem.* **2000**, *65*, 7919–7929.
 (43) Taniguchi, M.; Ra, D.; Mo, G.; Balasubramanian, T.; Lindsey, J. S. *J. Org. Chem.* **2001**, *66*, 7342–7354.
 (44) Mettath, S.; Li, G.; Srikrishnan, T.; Mehta, R.; Grossman, Z. D.; Dougherty, T. J.; Pandey, R. K. *Org. Lett.* **1999**, *1*, 1961–1964.
 (45) Senge, M. O.; Kalisch, W. W.; Runge, S. *Tetrahedron* **1998**, *54*, 3781–3798.

enantiomers in the asymmetric unit. (2) The saturated C–C bond (C(5)–C(6)) that fuses the five-membered ring to the porphyrin is significantly lengthened as compared to the corresponding C $_{\beta}$ –C $_{\beta}$ bonds on the other three purpurin pyrrole rings. (3) The pattern of alternating short and long C $_{\beta}$ –C $_{\beta}$ bond distances along the periphery of the macrocycle suggests significant conjugation between the porphyrin macrocycle and isocyclic ring.⁴⁶ Similar results have been observed for porphyrin derivatives with appended isocyclic six-membered rings.^{46,47} Insertion of Ni(II) into purpurin nitrile **8** followed by treatment with an excess of Weinreb's amide transfer reagent⁴⁸ under stringent conditions (90 °C for 3 days) yields the amidinium derivatized purpurin **9**. The Ni(II) complex is required for the application of Weinreb's reagent; the amide transfer reaction is not observed when the Zn(II) or free-base purpurin nitrile is used. Accordingly, target complex **1** is ultimately obtained upon demetalation of **9** followed by Zn(II) insertion.

Purpurin **7** is the branch point in the synthetic strategy en route to the chlorin amidinium (**2**). Catalytic hydrogenation of **7** with 10% Pd/C yields an intermediary porphyrinogen, which is reoxidized in air to yield the partially reduced macrocycle **10**. Selective reduction of the five-membered isocyclic ring of purpurin **7** is confirmed by mass spectrometry, which shows the addition of 1 equiv of molecular hydrogen. The ¹H NMR spectrum of **10** confirms that the integrity of the carbon skeleton is maintained upon reduction but lacks the signal attributable to a cyclopentenyl proton ($\delta \sim 9.20$ ppm). Following Ni(II) insertion to give **11**, reaction with Weinreb's reagent in a manner identical to that used to generate the homologous purpurin amidinium affords Ni(II) chlorin amidinium **12**. Demetalation followed by metalation with Zn(II) cleanly gives **2**.

The functionalization of the porphyrin periphery with a five-membered cyclopentenyl ring and its selective reduction provides a homologous set of porphyrin derivatives in which electronic communication between the proton transfer network and electron donor can be tuned with fidelity. This control over the electronic communication of the PCET pathway is in evidence from the pH dependence of the electronic absorption spectra of the Ni(II) purpurin and chlorin derivatives. The effect of deprotonation of the amidinium group of purpurin **9** on the UV–vis absorbance profile (Figure 2a) is pronounced. A hypsochromic shift is observed for the Soret band, which shifts from 436 nm for amidinium to 424 nm for amidine. Well-anchored isosbestic points are maintained at 434, 621, and 657 nm between the protonated (amidinium) and deprotonated (amidine) states of the proton interface. The blue shift in the Soret band is accompanied by similar spectral shifts in the Q-band region. By contrast, the absorption spectrum of chlorin **12** (Figure 2b) displays negligible shifts upon deprotonation of the amidinium functionality. The disparate behavior of the purpurin and chlorin spectral profiles illustrates the importance of conjugation in maintaining strong electronic coupling between the proton interface and porphyrin chromophore. Similar spectral changes have been observed for porphyrin Schiff base complexes, which exhibit 30-nm spectral shifts of both the Soret

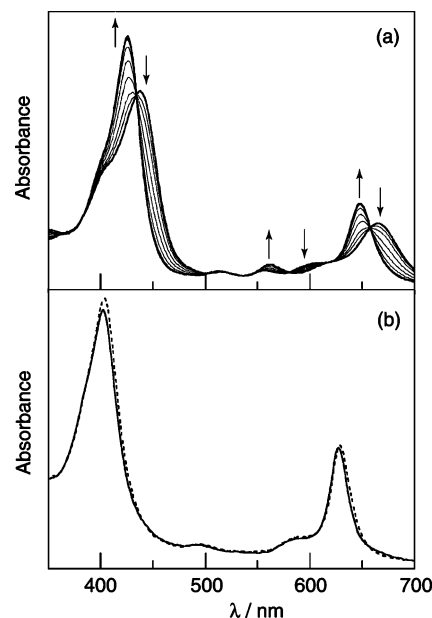


Figure 2. (a) Absorption spectra of amidinium purpurin **9** (0.80×10^{-6} M) in the presence of 0.00, 0.20, 0.40, 0.60, 0.80, 1.00, 1.40, 1.80, and 2.40 equiv of DBU in CH_2Cl_2 . Arrows indicate spectral changes upon addition of DBU. (b) Absorption spectra of chlorin **12** (0.90×10^{-6} M) in the absence (—) and presence (⋯) of 3.00 equiv of DBU in CH_2Cl_2 .

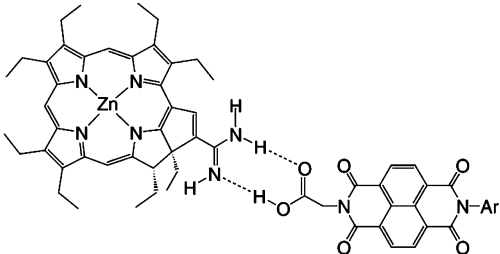
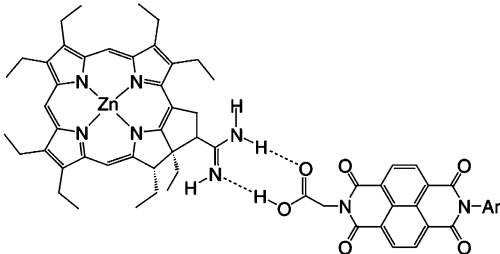
and Q-bands upon protonation.^{49–51} The red shift of the absorption maxima observed for both Schiff base porphyrins and the amidinium purpurin described here is ascribed to the resonance effect of the protonic electron-withdrawing group.⁵² Previous studies of porphyrin–amidinium conjugates have shown that when π -electron communication between chromophore and protonic group is interrupted, either by the presence of a saturated bridge or by canting of the amidinium out of the plane of the porphyrin π -system, absorbance shifts are negligible upon amidinium deprotonation.^{53,54} The results obtained for purpurin **9** and chlorin **12** reinforce these observations. Consistent with this spectroscopy, electronic structure calculations from density functional theory (DFT) show that orbital delocalization between the porphyrin macrocycle and the amidinium functionality is significant in purpurin **1**, but is minor in chlorin **2** (see Figures S1 and S2).

With the ability to couple and decouple the proton interface to the proximal ET pathway, the purpurin and chlorin provide a unique homologous pair for PCET investigations. PCET can be probed by replacing the Ni(II) center of **9** and **12** with Zn(II). The S_1 excited-state energy of Zn(II) purpurin **1** is 1.87 eV (298 K). Differential pulse voltammetry yields a one-electron reduction potential for amidinium donor **1** of $E_p(\text{I}^{2+/+}) = 1.02$ V vs Ag/AgCl in THF (Table 2). Purpurin **1** is emissive, and its excited state exhibits a monoexponential lifetime of $\tau = 1.90$ ns, which is attenuated slightly upon hydrogen bonding of the amidinium to the carboxylate of benzoate (**1**:benzoate) in THF

(46) Barkigia, K. M.; Thompson, M. A.; Fajer, J.; Pandey, R. K.; Smith, K. M.; Vicente, M. G. H. *New J. Chem.* **1992**, *16*, 599–607.
 (47) Arnold, D. P.; Gaete-Holmes, R.; Johnson, A. W.; Smith, A. R. P.; Williams, G. A. *J. Chem. Soc., Perkin Trans. 1* **1978**, 1660–1670.
 (48) Levin, J. I.; Turos, E.; Weinreb, S. M. *Synth. Commun.* **1982**, *12*, 989–993.

(49) Ward, B.; Callahan, P. M.; Young, R.; Babcock, G. T.; Chang, C. K. *J. Am. Chem. Soc.* **1983**, *105*, 634–636.
 (50) Petke, J. D.; Maggiora, G. M. *J. Am. Chem. Soc.* **1984**, *106*, 3129–3133.
 (51) Hanson, L. K.; Chang, C. K.; Ward, B.; Callahan, P. M.; Babcock, G. T.; Head, J. D. *J. Am. Chem. Soc.* **1984**, *106*, 3950–3958.
 (52) Ward, B.; Chang, C. K.; Young, R. *J. Am. Chem. Soc.* **1984**, *106*, 3943–3950.
 (53) Deng, Y.; Roberts, J. A.; Peng, S.-M.; Chang, C. K.; Nocera, D. G. *Angew. Chem., Int. Ed. Engl.* **1997**, *36*, 2124–2127.
 (54) Kirby, J. P.; van Dantzig, N. A.; Chang, C. K.; Nocera, D. G. *Tetrahedron Lett.* **1995**, *36*, 3477–3480.

Table 2. Thermodynamics and Kinetics for PCET for Purpurin and Chlorin Donor–Acceptor Complexes

PCET Dyads ^a	$E_p(\text{Donor})^{b,c}$	E_{0-0}^b	ΔG_{PCET}^d	k_{PCET}^b
 1:NI	1.02 V	1.87 eV	−0.47 V	$9.8 \times 10^8 \text{ s}^{-1}$
 2:NI	0.77 V	1.98 eV	−0.83 V	$9.5 \times 10^8 \text{ s}^{-1}$

^a Ar represents 2,5-di-*tert*-butylphenyl. ^b All data recorded in THF at 298 K. ^c $E_p(\text{Donor})$ is the $E_p(\mathbf{1}^{2+/+})$ and $E_p(\mathbf{2}^{2+/+})$ redox couples, which are referenced to SCE by using a ferrocenium/ferrocene internal standard of 0.307 V vs SCE. ^d $\Delta G_{\text{PCET}} = E_p(\text{Donor}) - E_{1/2}(\text{NI}^{-/2-}) - E_{0-0} + \Delta G(\epsilon)$, where $\Delta G(\epsilon)$ is the solvent reorganization energy, which in this case is estimated to be −0.14 eV based on geometrical parameters and choice of solvent. $E_{1/2}(\text{NI}^{-/2-}) = -0.52$ V vs SCE where NI^- is the carboxylate form of NI (see ref 69).

($\tau = 1.80$ ns). Conversely, the emission of **1** is quenched significantly when the benzoate is replaced by a naphthalenediimide (NI) electron acceptor bearing a carboxylate group, which has been successfully incorporated into previously studied D- -[H⁺]- -A assemblies.⁷ The one-electron reduction potential for this diimide acceptor has been measured to be $E_{1/2}(\text{NI}^{-/2-}) = -0.52$ V vs Ag/AgCl in THF (Table 2). Addition of the NI acceptor to a solution of purpurin **1** gives rise to biexponential decay kinetics with the shorter component arising from the supramolecular dyad **1:NI** ($\tau(\mathbf{1:NI}) = 0.65$ ns) and the longer component from unbound **1**. Analysis of the relative contributions of the bound and unbound lifetime components to the biexponential decay as a function of the total concentration of NI and **1** yields the formation constant from the following:

$$K_a = \frac{Q(Q+1)}{([\text{NI}]_0(Q+1) - [\mathbf{1}]_0Q)} \quad (1)$$

where Q is the ratio of the pre-exponential factors of the short and long components, which corresponds to $[\mathbf{1:NI}]/[\mathbf{1}]$. From the decay trace, $K_a(\mathbf{1:NI}) \approx 9.4 \times 10^3 \text{ M}^{-1}$ in THF. The observed quenching is attributed to ET from the S_1 excited state of **1** to the NI acceptor via the [H⁺] interface. This assignment is supported by the availability of 0.47 V driving force for ET (see Table 2), the absence of spectral overlap for resonant energy transfer,⁵⁵ and by comparison with previous studies whereby the charge-separated state involving a Zn(II) porphyrin–amidinium donor and the same NI acceptor was observed by transient absorption spectroscopy.⁷ The unimolecular rate constant for PCET in **1:NI** is determined to be $k_{\text{PCET}} = 9.8 \times$

10^8 s^{-1} , where k_{PCET} is determined from the difference of reciprocal lifetimes; $k_{\text{PCET}} = 1/\tau(\mathbf{1:NI}) - 1/\tau(\mathbf{1:benzoate})$. This calculation employs the natural lifetime of **1:benzoate** instead of **1** alone in order to account for the slight perturbation to the S_1 lifetime that is associated with amidinium–carboxylate binding, even in the absence of a redox-active quencher.

Similar results are observed for the Zn(II) amidinium chlorin complex (**2**), for which the S_1 excited-state energy is 1.98 eV (298 K) and one-electron reduction potential $E_{1/2}(\mathbf{2}^{2+/+}) = 0.77$ V vs Ag/AgCl in THF (Table 2). The monoexponential decay of the chlorin excited state increases slightly upon formation of the [H⁺] interface incapable of supporting ET ($\tau(\mathbf{2}) = 1.15$ ns, $\tau(\mathbf{2:benzoate}) = 1.20$ ns in THF). Addition of NI to **2** yields a biexponential decay curve as a result of the presence of unbound **2** and the dyad **2:NI**. Application of eq 1 to the biexponential decay yields $K_a \approx 1.3 \times 10^4 \text{ M}^{-1}$ in THF. The fast decay component has a lifetime of $\tau = 0.56$ ns to yield a rate constant $k_{\text{PCET}} = 9.5 \times 10^8 \text{ s}^{-1}$ for **2:NI** charge transfer.

The spectral signatures accompanying protonation/deprotonation of the amidine/amidinium in purpurin **9** provides a spectroscopic observable that can be used to determine pK_a . Titration of the amidinium purpurin in CH₃CN with the base DMAP produces the spectral series shown in Figure 2a. A Benesi–Hildebrandt plot of the spectral shifts (see Figure S3) yields a deprotonation constant (K_a'), which allows for the pK_a of purpurin **9** to be determined by the relation

$$pK_a(\mathbf{9}) = pK_a(\text{DMAP}) - \log(K_a') \quad (2)$$

The pK_a of DMAP in CH₃CN is 12.33,⁵⁶ yielding a $pK_a =$

(55) NI does not exhibit any absorption features at $\lambda > 400$ nm, which rules out resonant energy transfer from the purpurin/chlorin excited states.

(56) Izutsu, K. *Acid–base Dissociation Constants in Dipolar Aprotic Solvents*; Blackwell Scientific: Cambridge, MA, 1990.

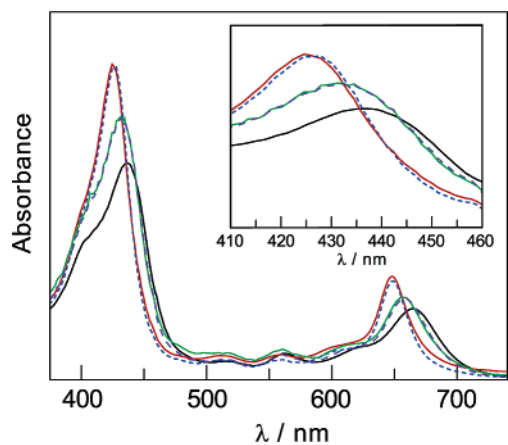


Figure 3. Absorption spectra of protonated purpurin **9** (0.63×10^{-6} M) (black, solid line, $\lambda_{\max} = 436$ nm), deprotonated purpurin **9** (red, solid line, $\lambda_{\max} = 424$ nm), and purpurin **9** upon addition of a large excess of benzoate (8.5×10^{-2} M) (blue, long dashed line, $\lambda_{\max} = 424$ nm), phenyl sulfonate (4.0×10^{-2} M) (green, solid line, $\lambda_{\max} = 432$ nm), and 3,5-dinitrobenzoate (3.12×10^{-4} M) (purple, long dashed line, $\lambda_{\max} = 432$ nm) in CH_2Cl_2 .

9.55 ± 0.10 for the ground state of amidinium purpurin **9**. The excited state ($[\text{AH}^+]^*$) is predicted to be a weaker acid than the ground state since the absorption spectrum of the conjugate base displays a hypsochromic shift relative to that of the conjugate acid ($h\nu_1 < h\nu_2$).^{57–60} The excited-state acidity constant, pK_a^* , is expressed by⁶¹

$$pK_a^* = \Delta G_a^*/2.3RT = pK_a - (h\nu_1 - h\nu_2)/2.3RT \quad (3)$$

For eq 3, $h\nu_1$ and $h\nu_2$ represent the energies of the 0–0 electronic transitions for the conjugate acid and base, respectively. Analysis of the electronic absorption and emission spectra corresponding to amidinium purpurin **9**, along with the corresponding deprotonated amidine, leads to the determination of $pK_a^* = 10.40 \pm 0.1$ in CH_3CN at 23 °C. These results demonstrate that upon excitation, **9** is nearly 10 times more basic than in the ground state ($pK_a = 9.55 \pm 0.1$). For the homologous electronically decoupled chlorin (**12**), virtually no change in acidity is observed upon excitation, as reflected by the invariance of the chlorin absorption profile as a function of protonation state (Figure 2b).

The spectra of amidine and amidinium purpurin **9** (Figure 2a) provide reference points for the direct evaluation of the nature of the hydrogen-bonding interface formed from the association of the donor to carboxylic acid and carboxylate acceptors, respectively, of varying pK_a 's. Figure 3 shows a series of spectra for amidinium **9** associated to benzoate, 3,5-dinitrobenzoate (DNB) (2,4-DNB gives the same result and is not shown for the sake of clarity), NI carboxylate, and phenyl sulfonate (PS). The absorption spectra of **9**:benzoate and **9**:NI assemblies more closely match that of **9** when it has been deprotonated with DMAP. Conversely, the absorption spectra of **9**:DNB and **9**:PS are red-shifted considerably from the amidine and display maxima that approach that of amidinium **9**. Some deviation from the spectrum of amidinium **9** is to be

expected to result from association, even if it is an ionized salt bridge. Comparison of these spectra leads to the conclusion that the $[\text{H}^+]$ interface is best described as an amidine–carboxylic acid when the acceptor is NI and as an amidinium–carboxylate/sulfonate salt bridge when **9** is bound to DNB/PS, respectively.

Discussion

The installation of an amidinium moiety on the porphyrin macrocycle permits the formation of supramolecular D– $[\text{H}^+]$ –A systems for the study of PCET. Interaction of an amidinium group with a carboxylate yields a stable and directional two-point hydrogen bond,⁶² making it an effective interface for the assembly of PCET supramolecular networks.^{7–10,63–66} The structural form of the $[\text{H}^+]$ interface, whether it exists as an amidinium–carboxylate or an amidine–carboxylic acid, has generally remained ill-defined. Aqueous pK_a values of typical amidinium salts ($pK_a \approx 11$ – 12)⁶⁷ and carboxylic acids ($pK_a \approx 5$ – 6)⁶⁷ suggest that an amidinium–carboxylate salt bridge is favored as shown in Chart 1 (left). On this basis, it has been assumed in PCET studies that salt-bridge formation is preferred and that charge transfer occurs across an interface possessing the large ionic component and strong dipole interaction engendered by the salt bridge (Chart 1, left). The ability to maintain electronic conjugation between the interface and the chromophoric core of purpurin **1** allows this supposition to be assessed directly. The measured pK_a of the amidinium purpurin ($pK_a = 9.55 \pm 0.10$ in CH_3CN) reveals that the amidinium is considerably more acidic than carboxylic acids such as benzoic acid, acetic acid, and dinitrobenzoates (2,4- and 3,5-) in organic solvents such as CH_3CN (pK_a values of 20.1, 22.3, and 16.1 in CH_3CN , respectively⁵⁶). Even relatively electron deficient acids such as trifluoroacetic acid ($pK_a = 12.65$ in CH_3CN ⁵⁶) have relatively high acidity constants in organic solvents. However, the pK_a values for amidinium and carboxylate do not solely determine the structure of the interface. Electrostatic energies that are specific to the interface must also be considered. For example, the $\Delta pK_a \approx 10$ between amidinium and carboxylate for **9**:benzoate in CH_3CN favors the amidine–carboxylic acid form of the interface by ~ 0.6 eV. A simple electrostatic calculation for a positive and negative charge at a salt-bridge distance of 3.9 \AA ⁷ in THF, however, translates to a stabilization energy of -0.50 eV, which nearly offsets the stabilization of the amidine–carboxylic acid tautomer derived solely from consideration of the ΔpK_a . Owing to the difficulty in predicting the net balance of these opposing energies, experimental tools that permit the location of the proton in the interface are essential. Purpurin **9** provides such a tool in its association to carboxylate acceptors of varying pK_a 's.

Amidines readily bind to a range of conjugate binding partners. In the case of carboxylic acids, the electron-deficient dinitrobenzoic acid is sufficiently acidic that it protonates the

(57) Ireland, J. F.; Wyatt, P. A. H. *Adv. Phys. Org. Chem.* **1976**, *12*, 131–160.
 (58) Shizuka, H. *Acc. Chem. Res.* **1985**, *18*, 141–147.
 (59) Arnaut, L. G.; Formosinho, S. J. J. *Photochem. Photobiol. A* **1993**, *75*, 1–20.
 (60) Tolbert, L. M.; Solntsev, K. M. *Acc. Chem. Res.* **2002**, *35*, 19–27.
 (61) Weller, A. Z. *Electrochemistry* **1952**, *56*, 662–668.

(62) Pranata, J.; Wierschke, S. G.; Jorgensen, W. L. *J. Am. Chem. Soc.* **1991**, *113*, 2810–2819.
 (63) Papoutsakis, D.; Kirby, J. P.; Jackson, J. E.; Nocera, D. G. *Chem. Eur. J.* **1999**, *5*, 1474–1480.
 (64) Otsuki, J.; Iwasaki, K.; Nakano, Y.; Itou, M.; Araki, Y.; Ito, O. *Chem. Eur. J.* **2004**, *10*, 3461–3466.
 (65) Camiolo, S.; Gale, P. A.; Ogden, M. I.; Skelton, B. W.; White, A. H. *J. Chem. Soc., Perkin Trans.* **2001**, *2*, 1294–1298.
 (66) Terfort, A.; von Kiedrowski, G. *Angew. Chem., Int. Ed. Engl.* **1991**, *5*, 654–656.
 (67) Smith, M. B.; March, J. *March's Advanced Organic Chemistry*, 5th ed.; John Wiley: New York, 2001.

Table 3. Summary of the Nature of the [H⁺] Interface in Dyads of **9**

binding moiety	salt bridge	nonionized
2,4-DNB	×	
3,5-DNB	×	
phenyl sulfonate	×	
benzoate		×
NI		×

amidine, as evidenced by the red shift of the Soret and Q-bands in Figure 3. The opposite is true for benzoic acid, establishing that the electron-withdrawing dinitro groups are important for the formation of the amidinium–carboxylate interface. In the case of phenyl sulfonate, the sulfonic acid group is sufficiently more acidic than the carboxylic group that salt-bridge formation prevail, even in the absence of electron-withdrawing groups on the phenyl ring (Table 3). These results are consistent with previous PCET studies of supramolecules formed from the association of a [Ru(bpy)₃]²⁺ donor (De) to a 3,5-dinitrobenzene acceptor (Ae) via amidinium–carboxylate and carboxylate–amidinium hydrogen-bonding interfaces; the salt bridge was assumed to form on the basis of aqueous pK_a's.^{8,10} The rate constant for PCET in the De–[amidinium–carboxylate]–Ae system is roughly 40 times slower than that for the De–[carboxylate–amidinium]–Ae complex. The large difference in PCET kinetics observed upon reversal of the asymmetric hydrogen-bonding interface was ascribed to the direction of ET relative to the orientation of the salt bridge. For De–[amidinium–carboxylate]–Ae, the direction of the salt-bridge dipole is in the direction of PCET; however, for the switched interface system, De–[carboxylate–amidinium]–Ae, the salt-bridge dipole opposes the direction of charge transfer. Accordingly, these results strongly implicated an ionized amidinium–carboxylate salt bridge. The spectroscopic results reported here for purpurin **1** support this assertion when the acceptor is acidic, as is the case for a dinitrobenzene carboxylic acid. Conversely, for electron-rich acceptors the situation is reversed. The non-ionized, amidine–carboxylic acid tautomer (Chart 1, right) is preferred for the NI acceptor. Accordingly, examination of assembly **1:NI** affords an assessment of the PCET kinetics for transport through a nonionized bridge. Moreover, its comparison to **2:NI** permits PCET kinetics to be compared for a D–[H⁺]–A assembly in which electronic communication between the proton interface and electron donor–acceptor sites is turned on and off. For these reasons, a comparative rate study of **1:NI** and **2:NI** was undertaken.

Rate expressions for PCET and ET reactions consist of nuclear (Franck–Condon) and electronic coupling (V_{el}) terms:

$$k \approx |V_{el}|^2 \text{FC} \quad (4)$$

Understanding the PCET kinetics of **1:NI** and **2:NI** requires the consideration of these terms separately. A direct kinetics comparison of **1:NI** and **2:NI** superficially involves electron transport along a PCET pathway that differs by only a π bond. We note, however, that the introduction of a double bond on the porphyrin periphery is not an innocent electronic perturbation. The π -conjugation of the purpurin delocalizes the donor electronic wave function more substantially onto the proton interface, as reflected by the disparate absorption changes observed for **9** as compared to **12** upon amidinium deprotona-

tion. We therefore infer that the electronic coupling between donor and acceptor for **1:NI** must be stronger than in **2:NI**. Similar variation in the electronic coupling has been observed for a single vs double bond situated one bond remote from a hydrogen-bonded interface.⁶⁸

In light of a larger V_{el} , which is presumed to exist for **1:NI** as compared with **2:NI**, it is puzzling that the rate for charge separation is virtually the same for both supramolecular dyads ($k_{\text{PCET}} = 9.8 \times 10^8 \text{ s}^{-1}$ for **1:NI** and $9.5 \times 10^8 \text{ s}^{-1}$ for **2:NI**). A relatively straightforward picture emerges for the PCET kinetics, however, upon consideration of the thermodynamics for the charge transfer processes of the two dyad systems. Although **1:NI** and **2:NI** are structurally similar, the chlorin is more easily oxidized. In addition, the chlorin excited state is higher in energy by ~ 0.1 V. Taken together, the driving force for PCET in **2:NI** is 0.35 V greater than that for PCET in **1:NI** ($\Delta G_{\text{PCET}}(\mathbf{1:NI}) = -0.47$ V; $\Delta G_{\text{PCET}}(\mathbf{2:NI}) = -0.83$ V).⁶⁹ When combining these values with an estimated reorganization energy of $\lambda \approx 1.1$ eV⁷⁰ for both systems and applying Marcus theory, we estimate that this difference in driving force results in a 17-fold smaller FC term for **1:NI** compared with **2:NI** at 298 K. Equation 4 suggests that the difference in the FC rate contributions could be canceled by ~ 4 -fold more favorable electronic coupling in **1:NI** compared with **2:NI**, which seems reasonable on account of the pronounced differences in electronic delocalization exhibited for **1** and **2**. Thus, the difference in electronic coupling is mitigated by thermodynamics of the PCET, leading to a situation in which the PCET kinetics for both supramolecular dyads are similar.

In summary, a set of homologous purpurin and chlorin derivatives appended with an amidinium functionality has been prepared. Electronic communication between the π -chromophore and appended amidinium in the purpurin has allowed for the structure of a [H⁺] interface in a D–[H⁺]–A assembly to be probed for the first time. For acidic acceptors, the amidinium–carboxylate salt bridge is preferred and PCET occurs through a D–[amidinium–carboxylate]–A assembly, as was inferred previously from directional PCET studies involving DNB carboxylic acids as acceptors.^{8,10} However, for acceptors bearing more electron density at the interface, such as NI, proton displacement from the carboxylic acid group is not pronounced and the assembly for PCET is better described as D–[amidine–carboxylic acid]–A. The position of the interfacial proton is thus sensitive to the peripheral electronic structure. Conjugation between the porphyrin chromophore and the amidinium interface can be altered by selective reduction of the isocyclic ring of an amidinium–purpurin to produce an amidinium–chlorin. A similar pK_a and nonionic interface structure is expected for the chlorin–amidinium, although

(68) Newton, M. D. *J. Electroanal. Chem.* **1997**, *438*, 3–10.

(69) This estimate includes the solvent-dependent Coulombic term ($\Delta G(\epsilon)$). Using the Born equation, we estimate an additional 0.14 eV toward the driving force for PCET in these systems in THF, based on a donor–acceptor distance of 14 Å and radii of 5 and 4 Å for the donor and acceptor, respectively.

(70) This estimate combines an outer-sphere reorganization energy of 0.85 eV (calculated using the Marcus dielectric continuum model for the systems in THF, based on a donor–acceptor distance of 14 Å and radii of 5 and 4 Å for the donor and acceptor, respectively) and an estimated inner-sphere contribution of 0.25 eV (based on previous reports that use similar electron donors and acceptors; see: Gaines, G. L., III; O'Neil, M. P.; Svec, W. A.; Niemczyk, M. P.; Wasielewski, M. R. *J. Am. Chem. Soc.* **1991**, *113*, 719–721).

electronic isolation of the amidinium from the porphyrin ring by virtue of the saturated isocyclic five-membered ring hinders direct measurement of the pK_a and interface structure. The interface is not significantly ionic, nor does the interface possess a significant dipole moment. Along these lines, a comparative study of the PCET kinetics for **1:NI** and **2:NI** reveals that contributions of the polarization to the PCET kinetics that are so dominant in salt-bridge assemblies are minimized in **1:NI** and **2:NI**. Instead, PCET through nonionized interfaces such as the amidine–carboxylic hydrogen-bonded bridge is largely dictated by electronic coupling.

Acknowledgment. The authors thank Dr. Yonqui Deng for initial synthetic work and Dr. Victor G. Young, Jr. for assistance in obtaining the X-ray crystal structure of **7**. J.R. thanks the

Fannie and John Hertz Foundation for a predoctoral fellowship. Financial support for this work was provided by the NIH (GM 47274).

Supporting Information Available: Spectral changes and Benesi–Hildebrand fit for titration of purpurin **9** with DMAP in CH_3CN , table of X-ray crystallographic data for complex **7** including a fully labeled thermal ellipsoid plot, final atomic coordinates, equivalent isotropic displacement parameters, anisotropic displacement parameters, and bond distances and angles. This material is available free of charge via the Internet at <http://pubs.acs.org>.

JA062430G